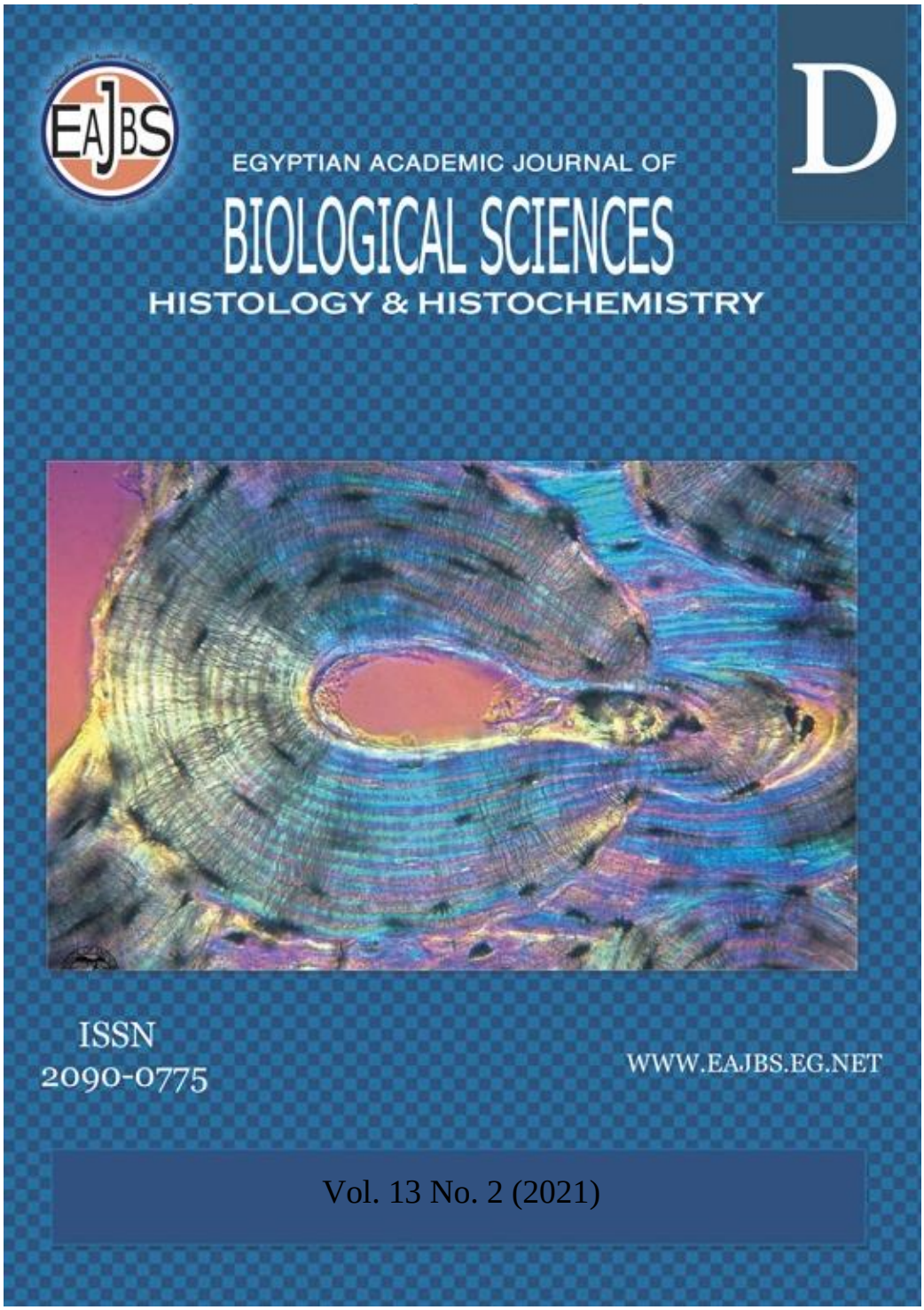

Citation: Egypt. *Acad. J. Biolog. Sci. (D-Histology and histochemistry) Vol.13(2) pp119-133(2021)*
DOI: 10.21608/EAJBSD.2021.205942

Egypt. Acad. J. Biolog. Sci., 13(2): 119-133 (2021)

Egyptian Academic Journal of Biological Sciences
D. Histology & Histochemistry
ISSN 2090 – 0775
http://eajbsd.journals.ekb.eg

Degenerative Changes in The Putamen of Growing Rats Induced by Maternal Excess Iron Exposure

Ayman S. Amer*, Mohamed N.M. Saleh, Mohamed El-Badry Mohamed and Omnia I. Ismail

Department of Human Anatomy and Embryology, Faculty of Medicine, Assiut University, Assiut, Egypt

E.Mail: ayman.amer@aun.edu.eg

ARTICLE INFO

Article History
Received:18/10/2021
Accepted:22/11/2021

***Keywords*:**
Putamen, Iron accumulation, Neuronal ultrastructure, Tyrosine hydroxylase immuno-histochemistry

ABSTRACT

Background: Iron is an essential element for all cells and plays important role in neurodevelopment. Putamen is the site of the highest iron concentration in the brain. Whether an elevated iron intake, might contribute to structural and cellular damage in the putamen or not remains currently unclear. **Aim of the Work:** To detect effects of high iron intake during the gestational and lactation periods on the putamen of offspring rats. **Material and Methods:** 16 pregnant rats were randomly equally divided into two groups; the control group received distilled water orally daily from the eighth day of pregnancy till the 20th day postnatally, and the treated group received ferrous gluconate dissolved in distilled water at a dose of 15 mg/kg body weight orally daily for the same period. Offspring rats included in this study were at the ages of newborn, 10 days, and 20 days. The brains from 6 male offspring from each age group were dissected, fixed, and processed for light microscopy, transmission electron microscopy, tyrosine hydroxylase immunohistochemistry, and morphometry. **Results:** The putamen in the three ages of the iron-treated group had vacuolations in the neuropil, and the neurons showed shrunken nuclei, vacuolations, damaged mitochondria with marked loss of cell organelles as compared to the control. Neurodegenerative changes were increased with increasing the age of rats. In addition, there was a reduction of positive TH immunoreactivity and a decrease in the cell count in the iron-treated group as compared to the control. **Conclusion:** Iron excess during pregnancy and lactation produced neuronal degeneration in the putamen of the growing rats.

INTRODUCTION

Iron supplementation during pregnancy is increasing to meet the nutritional demands of the pregnant women. There is essential role for iron; to form hemoglobin, to produce iron-sulfur proteins used in the oxidation process as in generating adenosine triphosphate, and to make iron-dependent enzymes needed to keep mitochondrial functions and healthy cellular milieu (Spence *et al.*, 2020). In the brain, iron contributes to the synthesis of myelin and neurotransmitters and is essential for normal neurological development (Fang *et al.*, 2018).

The putamen is a part of the dorsal striatum, and has been associated with learning, cognition, motor control, and language functions (Vinas-Guasch and Wu, 2017; De Deurwaerdere *et al*., 2020; Spence *et al.,* 2020). The putamen contains the highest levels of iron as compared to other regions of the brain (McAllum *et al.*, 2020).

Exposure to iron can occur due to ingesting a diet rich in iron, taking iron supplements, disorders of iron regulation proteins, several blood transfusions, hereditary hemochromatosis, or from occupational contact with iron dust as happens through soldering and in steel manufacturing (Crichton *et al.,* 2011; Weinreb *et al.,* 2013). Accumulation of iron is destructive and is associated with the production of free radicals that induce neuronal damage as in cases of type 2 diabetes mellitus (Li *et al.*, 2020), Alzheimer's (Matta *et al.,* 2017; Ayton *et al.,* 2021) and Parkinson's dementias (Thomas *et al.,* 2020), and Huntington's disease (Muller and Leavitt, 2014). Tyrosine hydroxylase (TH) is the key enzyme controlling the synthesis of dopamine in the putamen. Dopamine and other catecholamines play important roles as neurotransmitters and hormones. Although raised iron levels in the brain contribute to the pathogenesis of several disorders, it is unclear why neurodegeneration occurs only in specific brain nuclei while other iron-rich areas remain unaffected (Hare and Double, 2016).

In humans, even though iron is needed for fetal growth and development the provision of routine iron supplementation for pregnant women is a topic of debate (Jiang *et al.,* 2017). The neonatal period is perilous for the creation of normal iron content in the adult brain (Dal-Pizzol *et al.,* 2001). However, little research had been done to examine the cellular and structural changes that may occur in iron-overload states in the putamen of growing animals.

In this article, we observe the effects of increased maternal iron intake on the putamen of their offspring during the lactation period and examine the cellular ultrastructure of the putamen to identify whether any changes occurred and to what extent. This would help address the many important gaps in our understanding of this important topic and provide new insights into future research.

MATERIALS AND METHODS

Chemicals:

Iron (Fe^{2+}) was obtained from the CID company, Assiut, Egypt in the form of ferrous gluconate powder. Anti-tyrosine hydroxylase (TH) primary antibody and antipolyclonal secondary antibody universal kit were bought from the Sigma company (St. Louis, MO, USA).

Animals:

Sixteen healthy adult female albino rats (aged 3-4 months and 180-200g in weight) and eight adult male albino rats (aged 3-4 months and 200-250g in weight) were employed in this work. The animals were obtained from the Animal House Facility at the Faculty of Medicine, Assiut University, Egypt. Animals were maintained in metal cages at room temperature and 12:12hour light/dark cycle. The animals were fed with the standard rat chow and water ad libitum. All animals received humane care in compliance with the Animal Care Guidelines of the National Institutes of Health.

Experimental Design:

Female rats were mated with males (2:1) in each cage. The existence of sperms in the vaginal plug as seen by light microscopy was recorded as day 0 of pregnancy. The pregnant female rats were divided randomly into control and iron-treated groups (each consisted of 8 rats). The rats of the control group were given normal saline via gastric tube from the gestational day 8 through

parturition and lactation until weaning at postnatal day 20. Rats of the treated group received iron (ferrous gluconate) at a concentration of 15 mg/kg/day (Dal-Pizzol *et al.,* 2001) through a gastric tube for the same period. 6 male offspring rats from the control and treated groups were included in this study at the following ages (lactation period): newborn, 10 days, and 20 days. At the time of scarification, the rats were euthanized, subjected to intracardiac perfusion by normal saline 0.9% NaCl, followed by the fixative, and then sacrificed. Brain specimens were extracted from the rats, divided into two halves by a sagittal section, thereafter, coronal sections were made at the level of the mamillary body, and the area of the putamen and its surrounding structures were taken.

Light Microscopy:

Six brain specimens from each age group were fixed in 10% neutral-buffered formalin, dehydrated in ascending concentrations of alcohol, and cleared in xylene, then embedded in paraffin. 5-micron thick sections were prepared. The sections were stained with Einarson's Gallocyanine stain (Nissl's stain) according to a previous protocol (Suvarna *et al.,* 2019).

Transmission Electron Microscopy (TEM):

Brain specimens of six rats from each age group were fixed in 2.5% glutaraldehyde in sodium cacodylate buffer at pH 1.5 for 24 hours and then post-fixed in 1% osmium tetroxide for one hour (Kuo, 2014). The fixative was then washed out by distilled water and dehydration series were done. The specimens were embedded in fresh resin and incubated overnight at 60ºC. Semithin sections (one-micron thickness) were cut, stained with toluidine blue, and examined by light microscopy. Ultrathin sections (450–500 Aº) from selected areas were contrasted and stained with an alcoholic solution of uranyl acetate followed by aqueous lead citrate (Kuo, 2014), examined and photographed by the transmission electron microscope (JEOL Ltd. E.M.-100 CX11; Japan) at the Assiut University Electron Microscopy Unit.

Immunohistochemistry:

Immunostaining was done using the standard avidin-biotin peroxidase protocol (Goto *et al.,* 2015). Anti-Tyrosine hydroxylase (TH) immunohistochemical staining used as a marker for dopamine-producing neurons. After fixation in 10% neutral-buffered formalin for 2 days, brain specimens were dehydrated, cleared, and embedded in paraffin. 5-micron paraffin sections were prepared, mounted on coated slides, then placed in 10 mM sodium citrate buffer (pH 6.0) for 10 min to unmask antigens (Goto *et al.,* 2015). Brain sections were incubated in 0.3% H_2O_2 for 30 min to eliminate endogenous peroxidase activity. Slides were incubated with the primary antibody, 1:1000 polyclonal rabbit anti-TH (Gene Tex 113016, GeneTex, Inc. Company, Irvine, CA, USA), at 4°C for 18–20 hours, washed, and incubated with biotinylated secondary antibodies and then with the avidin-biotin complex. Thereafter, the sections were treated with 0.05% diaminobenzidine. Slides were then counterstained with Mayer's hematoxylin, dehydrated, cleared, and mounted. Negative control experiments were done by incubating the slides without the primary antibody; hence, no immunostaining occurred (Goto *et al.,* 2015). For positive control staining, the rat adrenal gland was immunostained as above and showed positive immunoreactivity for TH in the adrenal medulla, the positive cells appeared brown, and the nuclei were blue. All stained sections were inspected with an Olympus BX51 microscope, and images were captured by an Olympus DP72 CCD digital camera (Olympus Corporation, Tokyo, Japan).

Morphometric and Statistical Analysis:

The stained semithin sections were studied morphometrically for

measuring the number of the neurons per area (73680.4 μm²) in the putamen in both control and treated groups using computerized image analysis system software (Leica Q 500 MCO; Leica, Wetzlar, Germany) connected to a camera attached to a Leica universal microscope at Histology Department, Faculty of Medicine, Assiut University, Egypt. The data were collected from 6 animals in each age group. GraphPad Prism 5 (Graph Pad Software Inc., La Jolla, CA, USA) was used for data analysis. Data were presented as mean ± standard deviation (SD), and unpaired student's t-test was applied to compare between the two groups in each age. Differences of $P < 0.05$ were statistically significant.

RESULTS

Newborn Control Group:

By light microscopy, in the newborn control group, the caudate nucleus appears small, well-defined and lies on the floor of the lateral ventricle. It consists of densely stained neurons with minimum intercellular spaces. The putamen is larger in size than the caudate nucleus, well-defined, lies lateral to it, and is formed of densely stained neurons surrounded by perineuronal spaces and immature striatal fibers. The glial cells are smaller and darker than the neurons (Fig. 1A). Electron microscopy of the neurons of the putamen shows euchromatic nuclei, their cytoplasm shows rough endoplasmic reticulum, many free polyribosomes, and several scattered mitochondria (Fig. 2A). Using immunohistochemistry, the putamen shows strong positive TH immunoreactive neurons (Fig. 3A).

Newborn Treated Group:

The microscopic examination of the brain of the newborn treated group indicated that the caudate nucleus and the putamen are ill-defined in comparison with the control. The lateral ventricle appears dilated. The caudate nucleus is formed of packed deeply stained neurons and the intercellular spaces between the neurons are wider than that of the control. There is a separation between the caudate nucleus and the internal capsule. The putamen is formed of lightly stained neurons and the amount of Nissl granules is less than that of the control. The striatal fibers are not seen (Fig. 1B). The ultrastructure of the neurons of the putamen shows heterochromatic nuclei with ill-defined parts of the nuclear membranes. Vacuolations, few free polyribosomes, and a few scattered damaged mitochondria appear in the cytoplasm of the neurons, and the boundaries of the neurons are not seen (Fig. 2B). By immunohistochemistry, the putamen shows weaker positive TH immunoreactive neurons than that of the control (Fig. 3B).

Ten Days Old Control Group:

The histological examination of the brain in the 10 days old control group reveals that the caudate nucleus is a thin layer in the wall of the lateral ventricle, formed of deeply stained neurons with narrow intercellular spaces. On the other hand, the putamen is larger in size than the caudate nucleus and has well-defined lightly stained rounded neurons, vesicular nuclei, and narrow intercellular spaces. The glial cells are smaller and darker than the neurons (Fig. 4A). Transmission electron microscopy of the neurons of the putamen shows normal healthy histological structures (Fig. 5A). The immunohistochemistry indicated that the putamen has strong positive TH immunoreactive neurons (Fig. 6A).

Ten Days Old Treated Group:

The caudate nucleus and the putamen in the ten days old rats of the treated group are ill-defined and contain an amount of the Nissl′s granules less than that of the control. The lateral ventricle appears dilated. A separation between the putamen and the external capsule is evident. The caudate nucleus shows many vacuolations, wider intercellular spaces than that of the control, and neurons with dense nuclei and basophilic cytoplasm (Fig. 4B). Details of the neuronal cell structure in

the putamen show shrunken neurons with small-sized heterochromatic nuclei. The electron-dense cytoplasm shows many vacuolations, dilated rough endoplasmic reticulum, and a few free polyribosomes. Marked loss of cell organelles is observed (Fig. 5B). Immuno-expression of TH in the putamen shows a decrease in TH immunoreactivity with wide intercellular spaces between the neurons (Fig. 6B).

20 Days Old Control Group*:*

Light microscopic examination of the brain in the 20 days old control rats reveals that the caudate nucleus is very small, while the putamen is larger in size**.** The putamen shows neurons with vesicular nuclei and basophilic cytoplasm due to their content of Nissl's granules**.** Some neurons appear rounded, and others appear triangular. There are few blood vessels seen with normal endothelial cells. The striatal fibers, glial cells, and neuropil are noticed (Fig. 7A). The neuronal ultrastructure of the putamen shows normal histo-architecture (Fig. 8A). With the use of immunohistochemistry, the putamen shows strong positive TH immunoreactivity of the neurons, striatal fibers, and neuropil (Fig. 9A).

20 Days Old Treated Group:

Histological examination in the 20 days old treated group shows the caudate nucleus and the putamen as ill-defined structures containing fewer amounts of the Nissl′s granules compared to the control. The lateral ventricle is dilated. The putamen has shrunken neurons with darkly stained nuclei and irregular outlines. Some neurons show vacuolated cytoplasm, while others appear with lysis of the nuclei and dark cytoplasm. Many vacuolations are seen (Fig. 7B). Electron microscopic examination of the neurons of the putamen shows small-sized heterochromatic nuclei with peripheral condensation of the chromatin and indentation of the nuclear membrane. The cytoplasm shows many vacuoles, dilated rough endoplasmic reticulum, and destructed mitochondria (Figs. 8B). Studying the TH immuno-expression discloses that the putamen has a few positive TH immunoreactive neurons (Fig. 9B).

Morphometric and Statistical Study:

Newborn Rat Groups:

The number of cells in the putamen per an area of 73.680.4 μm² in the control group was 102.1 ± 1.4 (mean ± SD of 6 rats per group), while it was 90.6 ± 2.0 in the treated group as shown in (Fig. 10A). There was an insignificant decrease in the mean number of cells in the treated group as compared to the control ($p = 0.8$, unpaired student's t-test).

Ten Days Old Rat Groups:

The number of cells in the putamen per an area of 73.680.4 μm² in the control group was 81.6 ± 1.1 (mean ± SD of 6 rats per group), while it was 75.8 ± 1.7 in the treated group as shown in (Fig. 10B). There was an insignificant decrease in the mean number of cells in the treated group as compared to the control ($p = 0.6$, unpaired student's t-test).

20 Days Old Rat Groups:

The number of cells in the putamen per an area of 73.680.4 μm² in the control group was 61.8 ± 1.3 (mean ± SD of 6 rats per group), while it was 42.9 ± 1.8 in the treated group as shown in (Fig. 10C**).** There was a significant decrease in the mean number of cells in the treated group as compared to the control ($p = 0.002$, unpaired student's t-test).

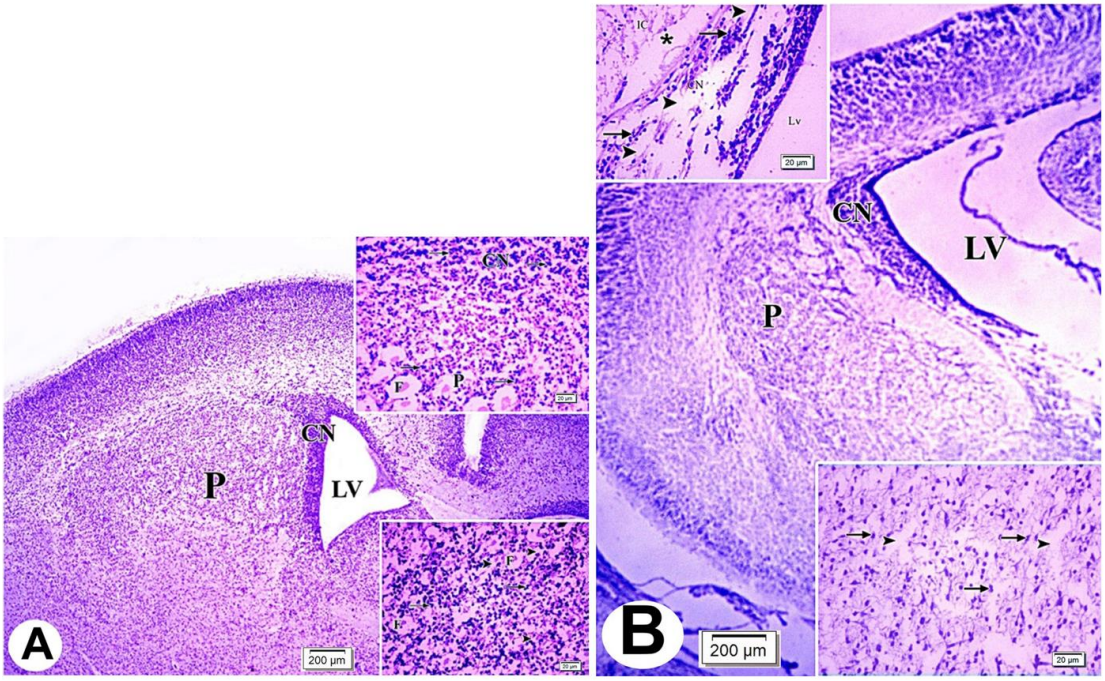

Fig. 1: Photomicrograph of coronal paraffin sections in the newborn rats' cerebral hemisphere. **A.** Control group showing the normal architecture; the caudate nucleus (CN) is small**,** well-defined and located in the floor of the lateral ventricle (LV). The putamen (P) is larger. **Inset above:** the caudate nucleus (CN) consists of dense neurons (arrow) with minimum intercellular spaces. The putamen (P) consists of dense neurons (arrow) and immature striatal fibers (F). **Inset below:** The putamen showing the dense neurons (arrow) surrounded by perineuronal spaces (arrowhead) and immature striatal fibers (F). **B.** Treated group showing the caudate nucleus (CN) and the putamen (P) are ill-defined. Notice apparently dilated lateral ventricle (LV). **Inset above:** the caudate nucleus (CN) consists of packed dense neurons (arrow) with wide intercellular spaces (arrowhead). There is a separation (asterisk) between CN and the internal capsule (IC). **Inset below:** the putamen showing the lightly stained neurons (arrow) have amount of Nissl′s granules less than that of the control, are surrounded by wide intercellular spaces (arrowhead). Gallocyanine, ×40 and Insets; Gallocyanine, ×400**.**

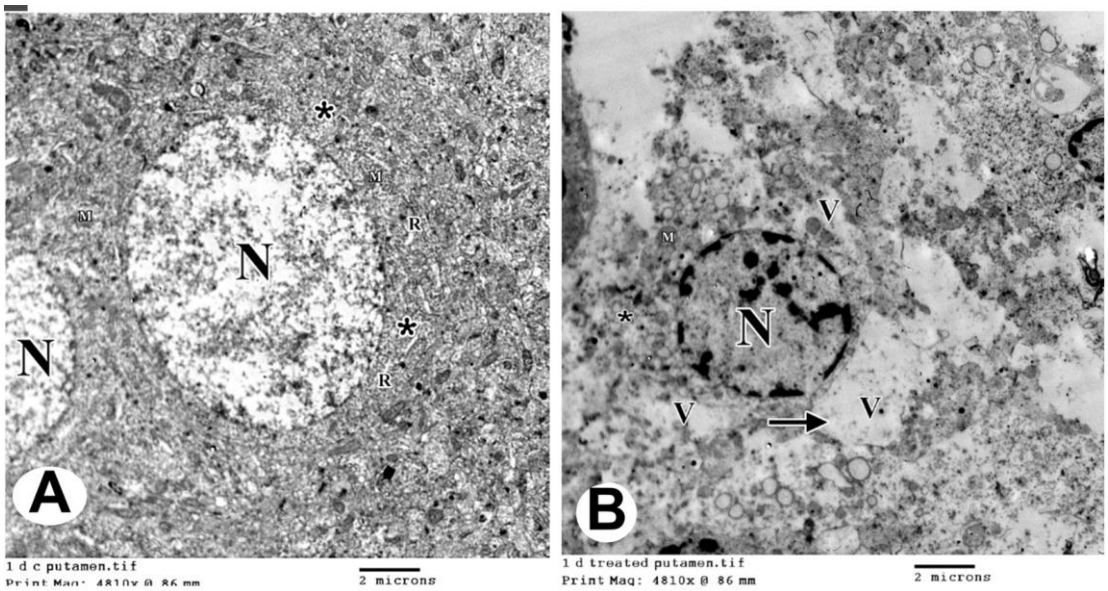

Fig. 2: Transmission electron micrograph of ultrathin sections in the newborn rats' putamen. **A.** Control group showing a neuron with an euchromatic nucleus (N) and a part of another neuron with its euchromatic nucleus (N). The cytoplasm shows rough endoplasmic reticulum (R), many free polyribosomes (asterisks) and scattered mitochondria (M). **B.** Treated group showing a neuron with small-sized heterochromatic nucleus (N). The cytoplasm shows many vacuolations (V) occupying a wide area (arrow), few polyribosomes (asterisk) and few mitochondria (M). The boundaries of the neuron are not seen. TEM, (**A,B**) ×4800.

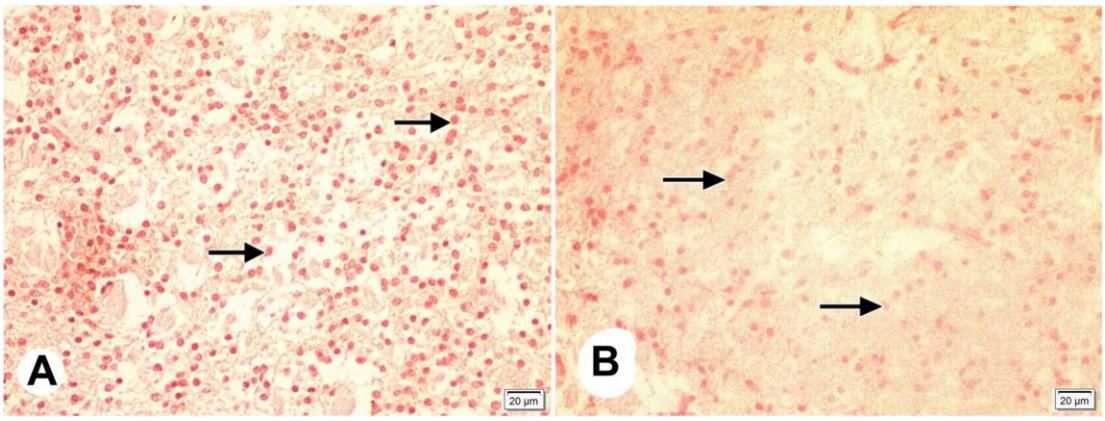

Fig. 3: Photomicrograph of tyrosine hydroxylase (TH) immunostaining in the newborn rats' putamen. **A.** Control group showing a strong positive TH immunoreactivity of neurons (arrows). **B.** Treated group showing the positivity of TH immunoreactive neurons is less than that of the control (arrows). TH immunostaining counterstained with Hematoxylin, ×400.

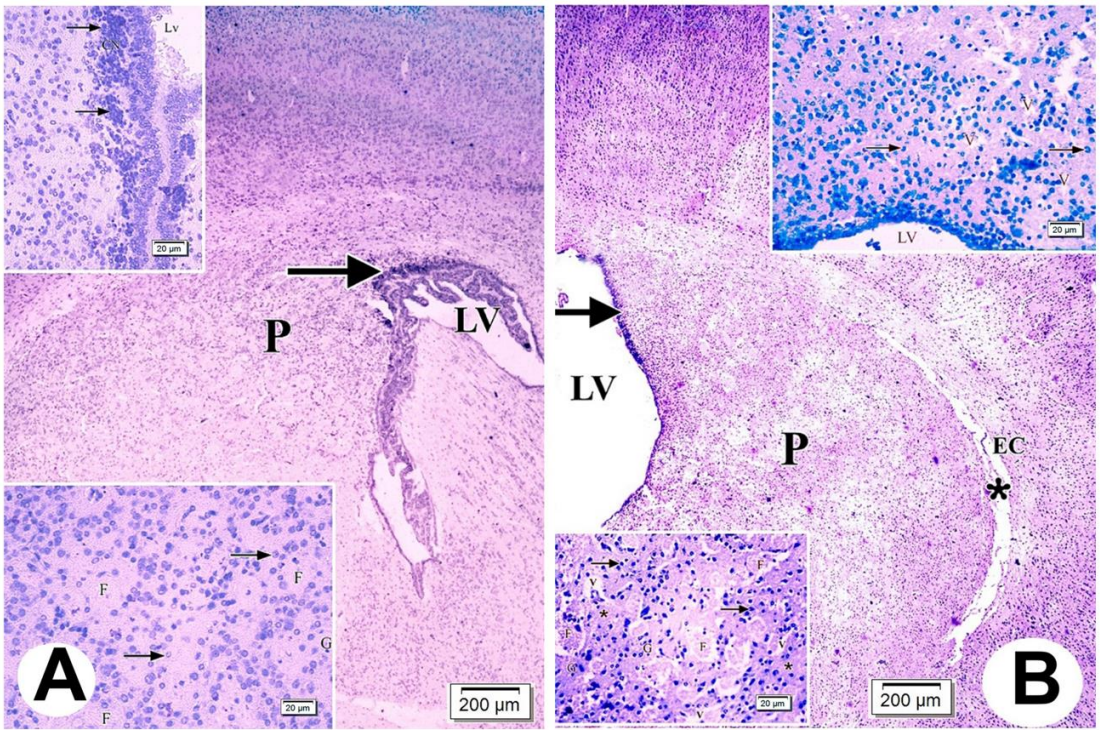

Fig. 4: Photomicrograph of coronal paraffin sections in the ten days old rats' cerebral hemisphere. **A.** Control group showing the healthy caudate nucleus (arrow) is seen as a thin layer in the floor of the lateral ventricle (LV) with narrow intercellular spaces. The putamen (P) is larger in size. **Inset above:** The caudate nucleus (CN) is formed of the deeply stained neurons (arrows). **Inset below:** The putamen consists of neurons (arrows) with vesicular nuclei. Notice the striatal fibers (F) and glial cells (G). **B.** Treated group showing the caudate nucleus (arrow) is seen as a thin layer with wide intercellular spaces. The putamen (P) is larger in size than the caudate nucleus, contains amount of the Nissl′s granules apparently less than that of the control, and appears ill-defined with wide intercellular spaces. There is a separation (asterisk) between the putamen and the external capsule (EC). Notice apparently dilated lateral ventricle (LV). **Inset above:** The caudate nucleus showing the neurons (arrows) have dense nuclei with vacuolations (V). **Inset below:** The putamen showing neurons (arrows) with dense nuclei and basophilic cytoplasm. The striatal fibers (F), glial cells (G), vacuolations (V) and neuropil (asterisks) are noticed. Gallocyanine, ×40 and Insets; Gallocyanine, ×400.

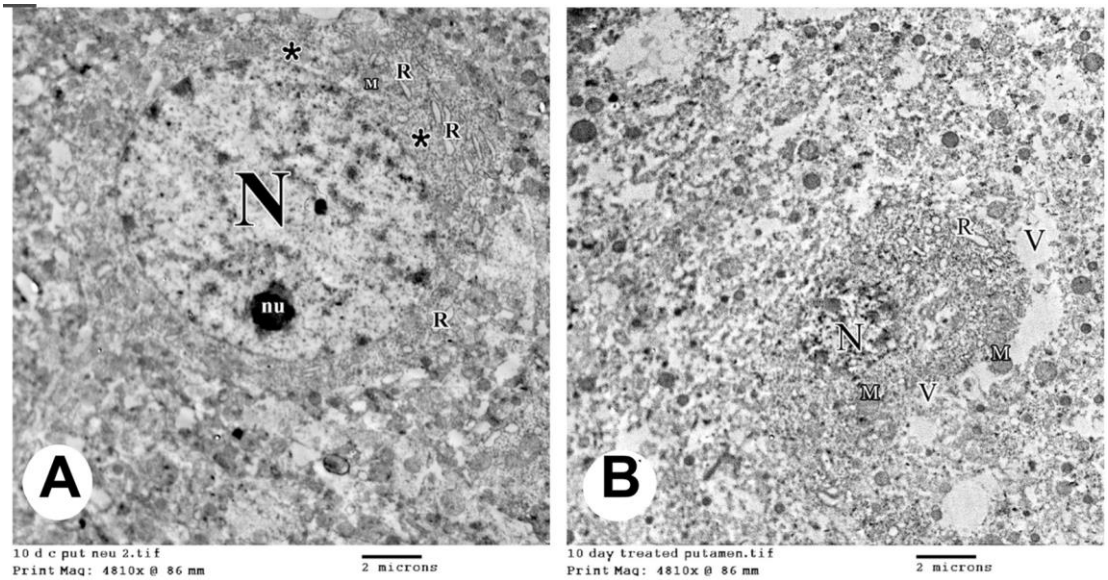

Fig. 5: Transmission electron micrograph of ultrathin sections in the ten days old rats' putamen. **A.** Control group showing a neuron with an euchromatic nucleus (N) and prominent nucleolus (nu). The cytoplasm shows rough endoplasmic reticulum (R), many free polyribosomes (asterisks) and scattered mitochondria (M). **B.** Treated group showing a shrunken neuron with small heterochromatic nucleus (N). The electron dense cytoplasm shows vacuolations (V), destructed mitochondria (M), and dilated rough endoplasmic reticulum (R). TEM, (**A,B**) ×4800.

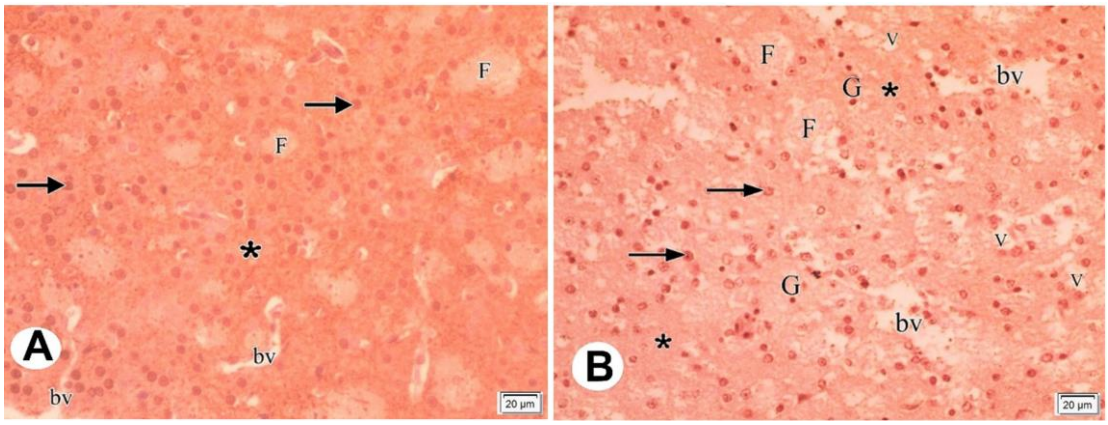

Fig. 6: Photomicrograph of TH immunostaining in the ten days old rats' putamen. **A.** Control group showing positive TH immunoreactive neurons (arrows). Notice the striatal fibers (F), blood vessels (bv), and neuropil (asterisk). **B.** Treated group showing apparently reduced number of positive TH immunoreactive neurons (arrows) with wide intercellular spaces. Dilated blood vessels (bv) are seen, and many vacuolations (V) are present. The striatal fibers (F), glial cells (G) and neuropil (asterisks) are noticed. TH immunostaining counterstained with Hematoxylin, ×400.

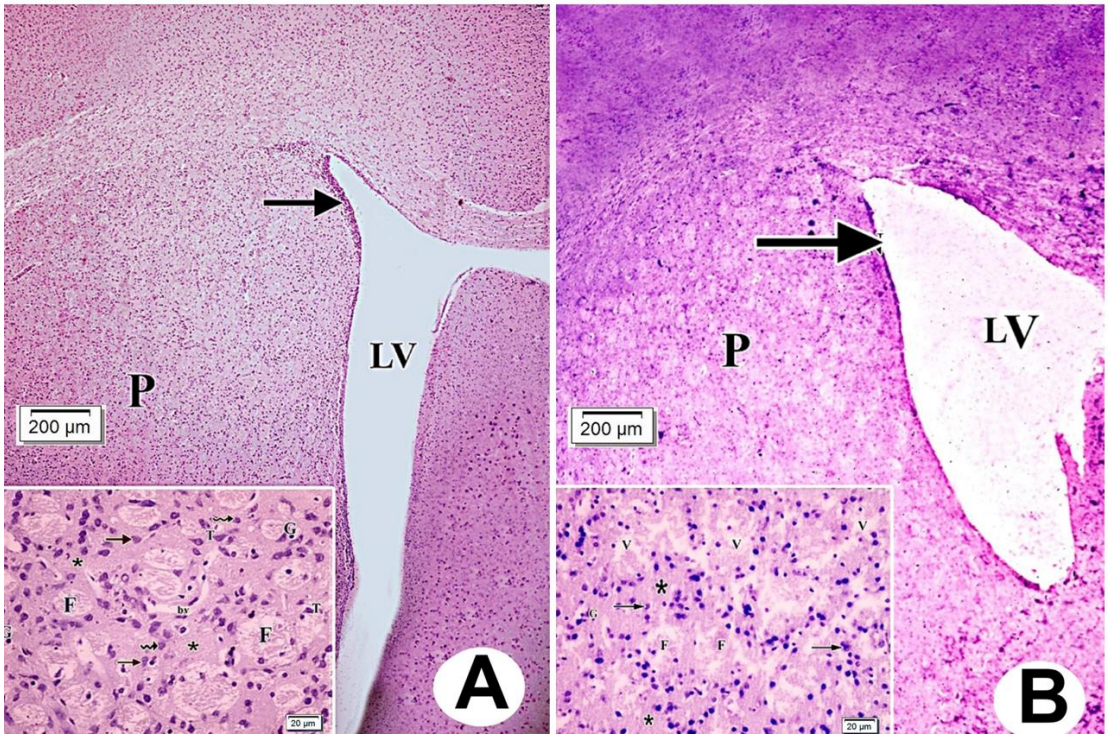

Fig. 7: Photomicrograph of coronal paraffin sections in the 20 days old rats' cerebral hemisphere. **A.** Control group showing the normal caudate nucleus (arrow) size is very small and lies on the floor of the lateral ventricle (LV). The putamen (P) is larger in size. **Inset:** The putamen shows neurons (arrows) with vesicular nuclei and basophilic cytoplasm. Some neurons appear rounded (wavy arrows) and others appear triangular (T). Blood vessels (bv), striatal fibers (F), glial cells (G), and neuropil (asterisks) are noticed. **B.** Treated group showing the caudate nucleus (arrow) is very small. The putamen (P) is larger, and ill-defined. Notice apparently dilated lateral ventricle. **Inset:** The putamen showing multiple neurons (arrows) with darkly stained nuclei. The striatal fibers (F), glial cells (G) and neuropil (asterisks) are noticed. Many vacuolations appear (V). Gallocyanine, ×40 and Insets; Gallocyanine, ×400.

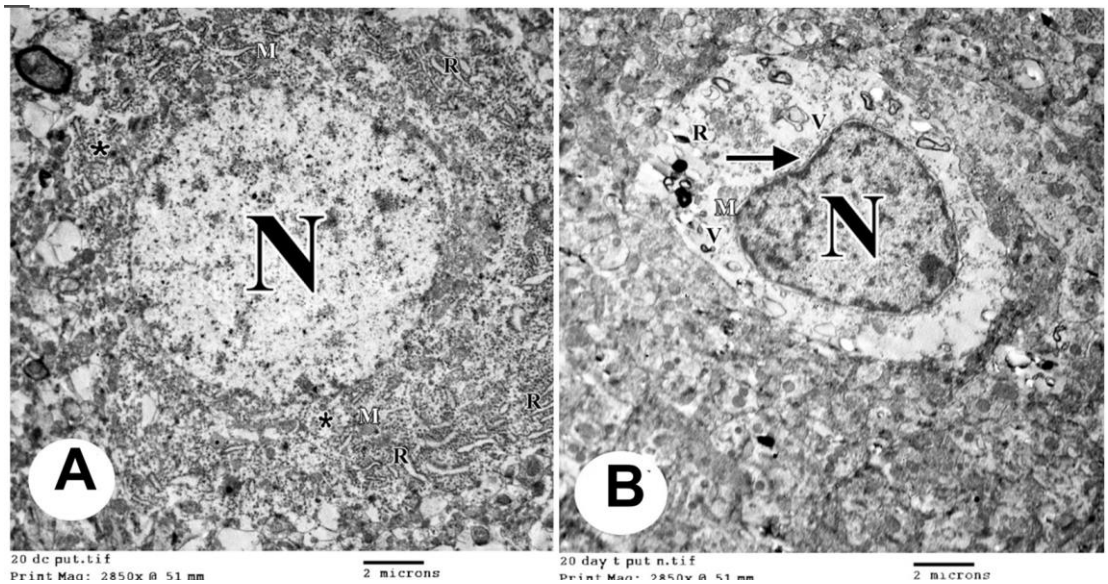

Fig. 8: Transmission electron micrograph of ultrathin sections in the 20 days old rats' putamen. **A.** Control group showing a neuron with an euchromatic nucleus (N). The cytoplasm shows rough endoplasmic reticulum (R), free polyribosomes (asterisks) and scattered mitochondria (M). **B.** Treated group showing a damaged neuron. The nucleus (N) has peripheral condensation of the chromatin with indentation of the nuclear membrane (arrow). The cytoplasm shows many vacuoles (V), dilated rough endoplasmic reticulum (R) and destructed mitochondria (M). TEM, (**A,B**) ×4800.

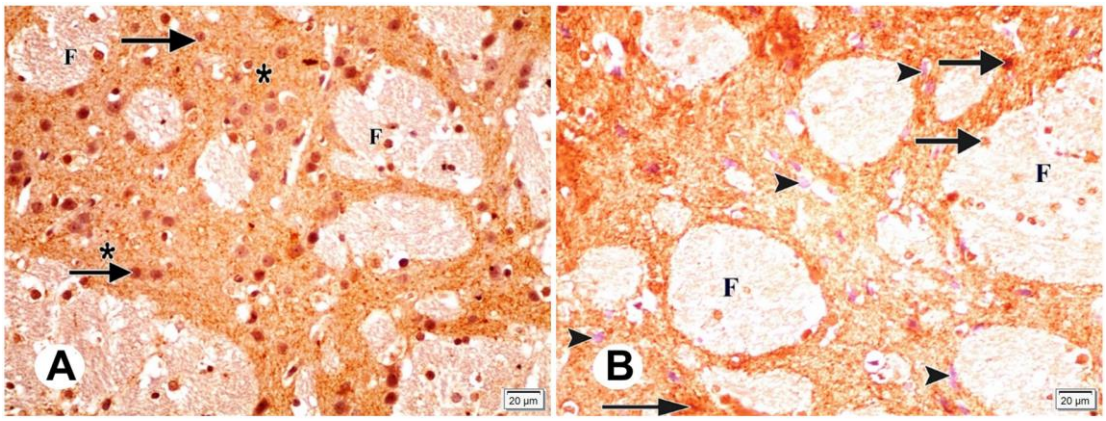

Fig. 9: Photomicrograph of TH immunostaining in the 20 days old rats' putamen. **A.** Control group showing a strong positive TH immunoreactivity of neurons (arrows), striatal fibers (F) and neuropil (asterisks). **B.** Treated group showing a few positive TH immunoreactive neurons (arrows) and many negative TH immunoreactive neurons (arrowheads). The striatal fibers (F) are noticed. TH immunostaining counterstained with Hematoxylin, ×400.

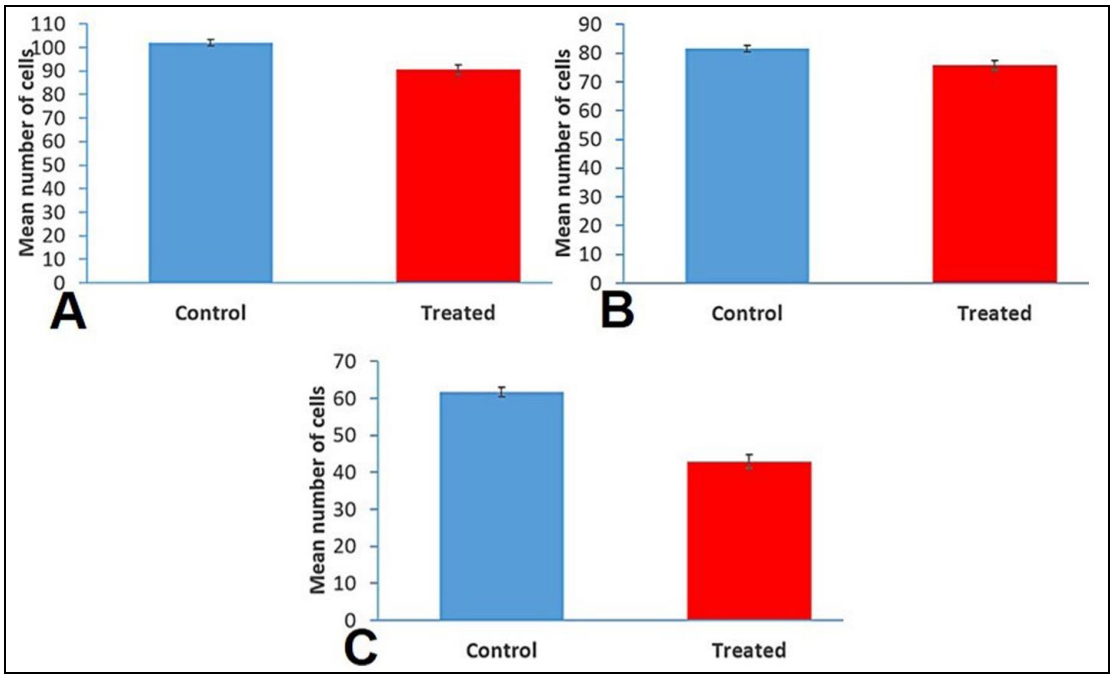

Fig. 10: Graphical representation showing the morphometrical results per an area of 73.680.4 µm² analyzed using GraphPad Prism Software version 5 (GraphPad Software Inc., La Jolla, CA, USA). **A.** Showing iron treatment decreased the mean number of cells in the putamen of newborn rats (not statistically significant difference as compared to the control, P = 0.8). **B.** Showing iron treatment decreased the mean number of cells in the putamen of ten days old rats (not statistically significant difference as compared to the control, P = 0.6). **C.** Showing iron treatment significantly decreased the mean number of cells in the putamen of 20 days old rats (with a statistically significant difference as compared to the control, P = 0.002).

DISCUSSION

Iron is indispensable for the normal functioning of the brain. Iron passes through the placenta to reach the fetus and passes through the mother's milk to the offspring (Crowe and Morgan, 1996). Iron also passes through blood-CSF and the blood-brain barriers to reach the central nervous system (Ariza *et al*., 2015; Qian and Ke, 2019). It is taken up by oligodendrocytes to help the formation of myelin, and by the nigrostriatal system to form tyrosine hydroxylase and dopamine (Hare and Double, 2016). The high level of iron uptake by the brain is acquired during the period of rapid brain growth in the first 3 weeks

of life in rats is related to the high level of transferrin receptors present in brain capillary endothelial cells in these animals (Crowe and Morgan, 1996). We have therefore undertaken this study to examine the consequences of excess iron exposure on the putamen during the suckling period of offspring rats.

In the current study, examination of the caudate-putamen of the newborn, 10 days, and 20 days old rats of both control and iron-treated groups was done. Light microscopy of brain specimens in all age groups revealed lateral ventricle dilatation in the iron-treated group as compared to the control. These findings agreed with those of Zhang *et al.* (2018) who found a marked lateral ventricle dilatation, brain edema and neurobehavioral disorder in iron-treated rats. They proposed that iron-induced oxidative stress products destroyed the ependymal cilia causing their shedding and stacking, which subsequently disturbed the normal cerebrospinal fluid circulation resulting in hydrocephalus (Zhang *et al.*, 2018). On the other hand, the apparent larger ventricular size in offspring of diabetic mothers could be a result of the reduction in the size of the striatum, not due to blockage of the drainage of the cerebrospinal fluid (Tehranipour *et al.*, 2009). More research is needed to clarify the cause of apparent large lateral ventricle size seen in the brains of the iron-treated group in our results.

In this study, light and electron microscopy of the putamen of newborns of the iron-treated group showed apparent increased intercellular spaces between the neurons in comparison with the control. The lateral ventricle appeared dilated, and there was a separation between the caudate nucleus and the internal capsule. These observations were in accordance with earlier researchers reporting brain edema due to iron excess (Zhang *et al.*, 2018). Electron microscopy of the neurons of the putamen revealed cellular degenerative changes as pyknotic nuclei, vacuolations, few free polyribosomes, and damaged mitochondria appeared in the cytoplasm. The present findings in the newborns of the iron-treated group might be attributed to the fact that the period of high iron uptake in the neonate corresponds with the onset of myelination performed by oligodendrocytes and is at risk of free radical-mediated injury since there is a relative deficiency of brain antioxidants, superoxide dismutase and glutathione peroxidase. This leads to the accumulation of hydrogen peroxide (H_2O_2) causing mitochondrial oxidative stress (Buonocore *et al.*, 2001).

In this work, light and electron microscopy of the putamen of 10 days and 20 days old rats of the iron-treated group displayed ill-defined putamen and caudate nucleus than that of the control. More damage was seen with increasing the age of the animals. Electron microscopy of the neurons of the putamen showed shrunken nuclei, many vacuolations, dilated rough endoplasmic reticulum, and marked loss of cell organelles. Our results were in line with those of Berggren *et al.* (2016) study that declared iron supplementation in neonatal mice resulted in striatal atrophy. The changes we observed in the iron-treated group in the present study might also be explained by Connor *et al.* (1995) who found that iron uptake and accumulation at the cellular level is highest during the postnatal period. Iron overload was associated with tissue damage due to its ability to mediate free radical production and lipid peroxidation (Crowe and Morgan, 1996). Moreover, the results of this study in the iron-treated group confirmed those of Saadeldien *et al.* (2012) study that found following iron intake there were neuronal and glial degenerations in the corpus striatum with iron deposition in the striatal tissue associated with changes indicative of cellular injury. They reported neuronal

apoptosis and necrosis, destruction of the organelles, including the mitochondria, endoplasmic reticulum, Golgi apparatus, and lysosomes of the neurons and glial cells.

In this research, we employed tyrosine hydroxylase (TH) immunohistochemistry since it is the main enzyme directing the synthesis of dopamine in the putamen. Dopamine and other catecholamines have vital roles as neurotransmitters and hormones. In the current study, immunohistochemistry of TH expression in the putamen of all ages of the iron-treated group showed a reduction in the TH immunoreactivity of neurons with increasing the age of rats, as compared to the control. These results were in harmony with other studies that showed progressive loss of the TH immunoexpression in the basal ganglia, elevated brain iron content and motor deficits with increasing the duration of their experiment (Minkley *et al.*, 2020). Furthermore, iron induces the breakdown of dopamine into toxic compounds that cause degeneration of the dopaminergic neurons in the putamen and nigrostriatal system as occurs in Parkinson's disease (Shehadeh *et al.*, 2019).

The morphometric study in this work showed an insignificant decrease in the number of neurons in the treated group as compared with the control at the ages of newborn and ten days while it showed a significant decrease at 20 days. Commensurate with the present results, Berggren *et al.* (2016) described that iron supplementation in the neonatal mice resulted in significantly decreased striatal neuronal cell body volumes and total striatal neuron numbers in the mature mice. The increased iron influx to the brain reacts with endogenously produced hydrogen peroxide from mitochondria to form hydroxyl radicals (Fenton reaction) (Muller and Leavitt, 2014). Nonetheless, iron causes oxidation of dopamine and the formation of neurotoxic products (Hare and Double, 2016), and causes eruptions in the wall of cellular organelles, inducing mitochondrial injury and apoptosis (Chan *et al.*, 2018). This further produces more hydroxyl radical species. The presence of iron and hydroxyl radicals, superoxides (reactive oxygen species), and reactive nitrogen species leads to increased lipid peroxidation, DNA damage, increased oxidative cellular stress, and eventually, neuronal toxicity and cell death through the iron-dependent cell death pathway termed ferroptosis (Nikseresht *et al.*, 2019).

Conclusions

Iron overdose during pregnancy and lactation produced structural deteriorations in the putamen of the growing albino rats. Therefore, strict control of the dose of iron intake during pregnancy and prevention of iron overload are recommended. Nonetheless, there are many questions that we cannot answer given our current knowledge. How iron interacts with other biomolecules; and how this coupling may be a viable target for the development of novel diagnostic and therapeutic approaches. This would be addressed in future research.

Conflicts of Interest: There are no conflicts of interest.

Ethics Approval: The experiments were approved by the Institutional Board Review and Ethics Committee of the Faculty of Medicine, Assiut University.

Financial Support and Sponsorship: Nil.

REFERENCES

Ariza J, Steward C, Rueckert F, Widdison M, Coffman R, Afjei A, *et al.* (2015). Dysregulated iron metabolism in the choroid plexus in fragile X-associated tremor/ataxia syndrome. *Brain Research*, 1598:88-96.

Ayton S, Portbury S, Kalinowski P, Agarwal P, Diouf I, Schneider JA, *et al.* (2021). Regional brain iron associated with deterioration in Alzheimer’s

disease: A large cohort study and theoretical significance. *Alzheimer's & Dementia*, 17:1244–1256.

Berggren KL, Lu Z, Fox JA, Dudenhoeffer M, Agrawal S, Fox JH. (2016). Neonatal iron supplementation induces striatal atrophy in female YAC128 Huntington's disease mice. *Journal of Huntington's Disease*, 5:53–63.

Buonocore G, Perrone S, Bracci R. (2001). Free radicals and brain damage in the newborn. *Biology of the Neonate*, 79(4): 180–186.

Chan S, Lian Q, Chen M-P, Jiang D, Ho JTK, Cheung Y-F, *et al.* (2018). Deferiprone inhibits iron overload-induced tissue factor bearing endothelial microparticle generation by inhibition oxidative stress induced mitochondrial injury and apoptosis. *Toxicology and Applied Pharmacology*, 338 :148-158.

Connor JR, Pavlick G, Karli D, Menzies SL, Palmer C. (1995). A histochemical study of iron-positive cells in the developing rat brain. *Journal of Comparative Neurology*, 355(1):111–123.

Crichton RR, Dexter DT, Ward RJ. (2011). Brain iron metabolism and its perturbation in neurological diseases. *Journal of Neural Transmission* 118: 301-314.

Crowe A, Morgan EH. (1996). Iron and copper interact during their uptake and deposition in the brain and other organs of developing rats exposed to dietary excess of the two metals. *The Journal of Nutrition*, 126(1):183-194.

Dal-Pizzol F, Klamt F, Frota Jr ML, Andrades ME, Caregnato FF, Vianna MM, *et al.* (2001). Neonatal iron exposure induces oxidative stress in adult Wistar rat. *Developmental Brain Research*, 130(1):109-114.

De Deurwaerdere P, Gaetani S, Vaughan RA. (2020). Old neurochemical markers, new functional directions?: An editorial for 'Distinct gradients of various neurotransmitter markers in caudate nucleus and putamen of the human brain' on page 650 *Journal of Neurochemistry*, 152(6):623-626.

Fang S, Yu X, Ding H, Han J, Feng J. (2018). Effects of intracellular iron overload on cell death and identification of potent cell death inhibitors. *Biochemical and Biophysical Research Communications*, 503(1):297-303.

Goto S, Morigaki R, Okita S, Nagahiro S, Kaji R. (2015). Development of a highly sensitive immunohistochemical method to detect neurochemical molecules in formalin-fixed and paraffin-embedded tissues from autopsied human brains. *Frontiers in Neuroanatomy*, 9:1–10.

Hare DJ, Double KL. (2016). Iron and dopamine: A toxic couple. Brain, 139:1026–1035.

Jiang H, Wang J, Rogers J, Xie J. (2017). Brain iron metabolism dysfunction in Parkinson's disease. *Molecular Neurobiology*,54:3078–3101.

Kuo J. (2014). Electron microscopy methods and protocols. New Jersey. Springer. Science & Business Media, CH 3, pp 1-19.

Li J, Zhang Q, Zhang N, Guo L. (2020). Increased brain iron deposition in the putamen in patients with type 2 diabetes mellitus detected by quantitative susceptibility mapping.

Journal of Diabetes Research, 2020:7242530.

Matta A, Cal H, Farinhas J, Masiero L, Teixeira S, Marinho V, *et al.* (2017). Iron accumulation and neurodegeneration in patients with Alzheimer's diseases: An integrative review study of the evidence. *EC Neurology*, 6(6): 267-272.

McAllum EJ, Hare DJ, Volitakis I, McLean CA, Bush AI, Finkelstein DI, *et al.* (2020). Regional iron distribution and soluble ferroprotein profiles in the healthy human brain. *Progress in Neurobiology*, 186:101744.

Minkley M, MacLeod P, Anderson CK, Nashmi R, Walter PB. (2020). Loss of tyrosine hydroxylase, motor deficits and elevated iron in a mouse model of phospholipase A2G6-associated neurodegeneration (PLAN). *Brain Research*, 1748:147066.

Muller M, Leavitt BR. (2014). Iron dysregulation in Huntington's disease. *Journal of Neurochemistry*, 130(3):328-350.

Nikseresht S, Bush AI, Ayton S. (2019). Treating Alzheimer's disease by targeting iron. *British Journal of Pharmacology*, 176:3622–3635.

Qian Z-M, Ke Y. (2019). Brain iron transport. *Biological Reviews*, 94:1672–1684.

Saadeldien HM, Mohamed AA, Hussein MRA. (2012). Iron-induced damage in corpus striatal cells of neonatal rats: attenuation by folic acid. *Ultrastructural Pathology*, 36(2):89-101.

Shehadeh J, Double KL, Murphy KE, Bobrovskaya L, Reyes S, Dunkley PR, *et al.* (2019). Expression of tyrosine hydroxylase isoforms and phosphorylation at serine 40 in the human nigrostriatal system in Parkinson's disease. *Neurobiology of Disease*, 130:104524.

Spence H, McNeil CJ, Waiter GD. (2020). The impact of brain iron accumulation on cognition: A systematic review *PLoS One,* 15(10):e0240697.

Suvarna SK, Layton C, Bancroft JD. (2019). Bancroft's theory and practice of histological techniques. 8th ed. Authors: S. Kim Suvarna, Christopher Layton and John D. Bancroft, Elsevier Ltd.

Tehranipour M, Khayyatzade J, Ghorbani Z. (2009). Maternal diabetes induced hydrocephaly in newborn rats. *Journal of Biological Sciences*, 9:625-628.

Thomas GEC, Leyland LA, Schrag A-E, Lees AJ, Acosta-Cabronero J, Weil RS. (2020). Brain iron deposition is linked with cognitive severity in Parkinson's disease. *Journal of Neurology, Neurosurgery and Psychiatry*, 91(4):418-425.

Vinas-Guasch N, Wu YJ. (2017). The role of the putamen in language: a meta-analytic connectivity modeling study. *Brain Structure and Function*, 222(9):3991-4004.

Weinreb O, Mandel S, Youdim MBH, Amit T. (2013). Targeting dysregulation of brain iron homeostasis in Parkinson's disease by iron chelators. *Free Radical Biology and Medicine*, 62:52-64.

Zhang J, Shi X, Chen Z, Geng J, Wang Y, Feng H, *et al.* (2018). Edaravone reduces iron-mediated hydrocephalus and behavioral disorder in rat by activating the Nrf2/HO-1 pathway. *Journal of Stroke and Cerebrovascular Diseases*, 27(12):3511-3520.

ARABIC SUMMARY

تغيرات تنكسية في البوتامين بالفئران النامية الناجم عن تعرض الأم للحديد الزائد

أيمن صلاح الدين عامر، محمد نبيل محمود صالح، محمد البدري محمد، أمنية إبراهيم محمد إسماعيل
قسم التشريح الآدمي وعلم الأجنة – كلية الطب –جامعة أسيوط

الخلفية: إن الحديد هو عنصر أساسي لجميع خلايا الجسم ، ويلعب دورًا مهمًا في نمو الجهاز العصبي. البوتامين هو المكان الذي يوجد فيه أعلى تركيز للحديد في الدماغ. ومن غير الواضح حاليًا ما إذا كان تناول الحديد المرتفع قد يساهم في حدوث تلف في تركيب وخلايا البوتامين أم لا.
الهدف من البحث: الكشف عن آثار تناول كميات كبيرة من الحديد خلال فترات الحمل والرضاعة على بوتامين الجرذان الصغيرة.
المواد والطرق المستخدمة: تم تقسيم 16 فأر حامل بشكل عشوائي إلى مجموعتين. تلقت المجموعة الضابطة الماء المقطر عن طريق الفم يومياً من اليوم الثامن من الحمل حتى اليوم العشرين بعد الولادة ، والمجموعة المعالجة تلقت جلوكونات حديدية مذابة في الماء المقطر بجرعة 15 مجم / كجم من وزن الجسم عن طريق الفم يومياً لنفس الفترة. كانت ذرية الجرذان المشمولة في هذه الدراسة في سن حديثي الولادة ، 10 أيام ، و 20 يومًا. تم تشريح المخ لعدد 6 ذكور من كل فئة عمرية ، وحفظه وتحضيره من أجل الفحص المجهري الضوئي ، والمجهر الإلكتروني النافذ ، والكيمياء المناعية للتيروزين هيدروكسيلاز ، وتم عمل دراسة مورفومترية - قياسات شكلية.
النتائج: كان البوتامين في الأعمار الثلاثة من المجموعة المعالجة بالحديد يحتوي على فجوات ما بين الخلايا ، وأظهرت الخلايا العصبية أنوية منكمشة ، وفراغات في السيتوبلازم ، وميتوكوندريا تالفة مع خسارة ملحوظة في عضيات الخلية مقارنة بالمجموعة الضابطة. وقد لوحظ زيادة التغيرات التنكسية العصبية مع زيادة عمر الفئران. بالإضافة إلى ذلك ، أظهرت دراسة الكيمياء النسيجية المناعية نقص الخلايا العصبية ذات النشاط المناعي الإيجابي TH وانخفاض ملحوظ في عدد خلايا البوتامين للمجموعة المعالجة بالحديد بالمقارنة مع المجموعة الضابطة.
الخلاصة: أدى التعرض الزائد للحديد أثناء الحمل والرضاعة إلى تنكس الخلايا العصبية في بوتامين الفئران النامية.